Journal of Wind Engineering & Industrial Aerodynamics 191 (2019) 41–53

Contents lists available at ScienceDirect

Journal of Wind Engineering & Industrial Aerodynamics

journal homepage: www.elsevier.com/locate/jweia

Numerical study of wind turbine wakes over escarpments by a modified delayed detached eddy simulation

Guo-Wei Qian, Takeshi Ishihara *

Department of Civil Engineering, School of Engineering, The University of Tokyo, 7-3-1, Hongo, Bunkyo-ku, Tokyo, Japan

ARTICLE INFO

Keywords:
Wind turbine wake
Modified delayed detached eddy simulation
Escarpment
Wake model

ABSTRACT

The wake of wind turbine in a complex terrain site is investigated by a modified delayed detached eddy simulation (MDDES) and a hybrid framework to predict the wind turbine wake effects in a real wind farm are presented. The wind field and turbine wake flows over the real terrain are simulated for different directions and validated by comparing with those measured by a LiDAR in the wind farm. Subsequently, the wake characteristics over the escarpment are systematically investigated by numerical simulations and the terrain effects on the turbine wake flow are clarified. A hybrid framework is then utilized for a wind farm over complex terrain. In this framework, the effects of local terrain and surface roughness on the wind speed, wind direction and turbulence intensity are taken into account by the numerical simulation, while the wind turbine wakes are represented by a new Gaussian-based analytical wake model. Finally, the applicability of the proposed framework is verified by comparison with the numerical simulation results of wake over the escarpment.

1. Introduction

The areas near the coastline are usually the locations for the onshore wind power plants because of the high wind speeds and low turbulence intensities in the ocean side. However, the coast areas in Japan are also often accompanied with complex terrains in the land side, thus the ambient turbulence varies considerably depending on wind direction (Ishihara et al., 2004). Another key aspect is the local terrain effects on the wind turbine wake behavior, which makes the wind power prediction more uncertain and wind farm layout design complicated than that for the flat terrain.

Wind turbine wakes over complex terrain involve different aspects, including wind prediction over terrain, boundary layer surface roughness modelling and wind turbine modelling. Extensively numerical studies by using Computational Fluid Dynamics (CFD) have been performed in this research field. In the early stage, the wake and terrain effects were superposed by linear models, where turbine wakes were calculated using the UPMWAKE model and flow over terrain was solved based on a linearization of equations, named UPMORO (Crespo et al., 1993; Migoya et al., 2007). By comparison with measurements in a real wind farm, the linearized wind flow models of UPMORO and WAsP were found to be able to provide acceptable results only for moderate complex terrain with attached flows (Migoya et al., 2007). Most of numerical investigations of the wake flow over complex terrain were conducted by the Reynolds-Averaged Navier-Stokes (RANS) equations with $k-\varepsilon$, $k-\omega$ and RSM turbulence closures (Daaou Nedjari et al., 2017; Makridis and Chick, 2013; Murali and Rajagopalan, 2017). However, as pointed by Ishihara and Qi (2019), the RANS models have some limitations for wind prediction over steep terrains with smooth surfaces, in which the mean wind speed was overestimated and the turbulent kinetic energy was underestimated since the organized motions behind a 3D smooth hill cannot be captured. Large Eddy Simulation (LES) was employed to study the terrain effects of an ideal 3D hill (Yang et al., 2015) and 2D ridge (Shamsoddin and Porté-Agel, 2017) for the model wind turbine wakes and it was found that turbine wakes downwind of the hill recover faster due to the enhanced turbulent transport. Berg et al. (2017) performed the LES to simulate wake flow over a real complex terrain and showed that a strong recirculation zone behind the ridge prevented the wake flow from following the terrain. LES requires very fine grids to resolve near-wall turbulent flows with high computational cost, thus a hybrid RANS/LES model is alternatively proposed, in which RANS acts on predicting the attached flow close to walls and LES works for capturing the detached flows on the lee side of steep terrains (Bechmann and Sørensen, 2010). The detached eddy simulation (DES) model blends RANS and LES model according to the idea of switching length scale in partial differential equations (Shur et al., 1999). Since the DES model exhibits incorrect

* Corresponding author.
E-mail address: ishihara@bridge.t.u-tokyo.ac.jp (T. Ishihara).

https://doi.org/10.1016/j.jweia.2019.05.004
Received 30 September 2018; Received in revised form 12 May 2019; Accepted 12 May 2019

behavior in thick boundary layers, Spalart et al. (2006) later proposed a new formulation of DES to preserve the RANS model throughout the boundary layer, which is known as the delayed detached eddy simulation (DDES). The evaluation for the terrain effects on turbines by using the DDES was carried out by Schulz et al. (2016), and they pointed out that the reduction of turbulence and the inclination flow over the escarpment directly affected the loads and power. However, these numerical simulations for the turbine wakes over real complex terrain are lack of validation by field measurements. In addition, the effects of terrain with different heights respect to the turbine have not been systematically investigated.

The optimization of wind farm involves a larger number of calculations, thus analytical wake models with low computational cost have advantages over the full CFD simulations. Recently, Shamsoddin and Porté-Agel (2018) developed an analytical model to predict the turbine wake flow over a two-dimensional hill of moderate slope and validated by the numerical simulations. However, wake flow over complex terrain with various roughness is still called into question for the engineering application. The common approach applied in complex terrain is a pure superposition of wake effects over the wind field over topography. Feng and Shen (2014) utilized the Jensen wake model (Jensen, 1983) to approximate the wake effects by taking the CFD simulated wind flow conditions as input and then applied to wind farm layout optimization on a Gaussian shape hill. However, as pointed by Hyvärinen and Segalini (2017), the Jensen wake model cannot accurately capture the wake characteristics over hills, and a wake model with sufficient accuracy is necessary for the commonly used superposition approach to yield reasonable results in complex terrain. Kuo et al. (2018) developed a numerical wake model for simulating wakes on complex terrains. The model solves a simplified variation of the Navier-Stokes equations with simplifications and assumptions to reduce computational cost. However, the wake modelling over the complex terrain was not validated, and the wake deflections induced by the local wind direction changes were not considered.

This study aims to investigate wind turbine wakes over the complex terrain by using a MDDES model and to verify the hybrid framework used for wind turbine wake predictions in complex terrain. In section 2, the numerical model used in this study is presented and validated by comparison with the field measurement. In section 3, the applicability of the hybrid framework for wake modelling in complex terrain is verified by the numerical simulations. Conclusions of this study are summarized in section 4.

2. Numerical model and validation

This section discusses the numerical model and its validation by field measurement. Firstly, the turbulence model, canopy model and wind turbine model utilized in this study are presented in section 2.1 and 2.2, respectively. The numerical setup including the computational domain, grid system and boundary condition are introduced in section 2.3. Section 2.4 describes the onshore test site and the measurement devices setup. The accuracy of the developed numerical model is validated in section 2.5 by comparing the predicted and measured turbine wake flows in a real wind farm.

2.1. Turbulence model

The finite volume method (FVM) is applied for the discretization of the governing partial differential equations. The continuity and momentum equations for incompressible flow are given by:

$$\frac{\partial \rho \tilde{u}_i}{\partial x_i} = 0 \tag{1}$$

$$\frac{\partial(\rho \tilde{u}_i)}{\partial t} + \frac{\partial(\rho \tilde{u}_j \tilde{u}_i)}{\partial x_j} = -\frac{\partial \tilde{p}}{\partial x_i} + \frac{\partial}{\partial x_j}\left[\mu\left(\frac{\partial \tilde{u}_i}{\partial x_j} + \frac{\partial \tilde{u}_j}{\partial x_i}\right)\right] + \frac{\partial \tau_{ij}}{\partial x_j} + f_{\tilde{u},i} \tag{2}$$

where $\tilde{u}_i$ is the resolved wind speed in the ith direction and $\tilde{p}$ is the resolved pressure. ρ is the density of the fluid, μ is the molecular viscosity and the source term $f_{\tilde{u},i}$ is the fluid force per unit grid volume. τ_{ij} is introduced to consider difference between $\widetilde{u_i u_j}$ and $\tilde{u}_i \tilde{u}_j$, i.e.

$$\tau_{ij} = -\rho\left(\widetilde{u_i u_j} - \tilde{u}_i \tilde{u}_j\right) \tag{3}$$

where $\widetilde{u_i u_j}$ represents the total Reynolds stress in the computational cell.

In order to close the governing equations, τ_{ij} is normally modelled following the eddy viscosity hypothesis, where τ_{ij} are assumed as products of the fluid strain and eddy viscosity.

$$\tau_{ij} = 2\mu_t \tilde{S}_{ij} + \frac{\delta_{ij}}{3}\tau_{kk}, \quad \tilde{S}_{ij} = \frac{1}{2}\left(\frac{\partial \tilde{u}_i}{\partial x_j} + \frac{\partial \tilde{u}_j}{\partial x_i}\right) \tag{4}$$

where $\tilde{S}_{ij}$ is the strain rate tensor, and μ_t is the eddy viscosity and is computed by the turbulence model. In the DDES model, μ_t is defined as:

$$\mu_t = \rho C_\mu \frac{\tilde{k}^2}{\tilde{\varepsilon}} \tag{5}$$

where the constant C_μ is 0.09, $\tilde{k}$ and $\tilde{\varepsilon}$ are the turbulent kinetic energy and the dissipation of turbulent kinetic energy respectively. The term $(\delta_{ij}/3)\tau_{kk}$ is absorbed into the pressure term (Bechmann and Sørensen, 2010). $\tilde{k}$ and $\tilde{\varepsilon}$ are obtained by solving additional two equations. In this study, the realizable $k-\varepsilon$ model is used and the transport equations for $\tilde{k}$ and $\tilde{\varepsilon}$ are:

$$\frac{\partial(\rho\tilde{k})}{\partial t} + \frac{\partial(\rho\tilde{k}\tilde{u}_i)}{\partial x_i} = \frac{\partial}{\partial x_j}\left[\left(\mu + \frac{\mu_t}{\sigma_k}\right)\frac{\partial \tilde{k}}{\partial x_j}\right] + G_k + Y_k \tag{6}$$

$$\frac{\partial(\rho\tilde{\varepsilon})}{\partial t} + \frac{\partial(\rho\tilde{\varepsilon}\tilde{u}_i)}{\partial x_i} = \frac{\partial}{\partial x_j}\left[\left(\mu + \frac{\mu_t}{\sigma_\varepsilon}\right)\frac{\partial \tilde{\varepsilon}}{\partial x_j}\right] + C_{\varepsilon 1} G_k \frac{\tilde{\varepsilon}}{\tilde{k}} - C_{\varepsilon 2}\rho\frac{\tilde{\varepsilon}^2}{\tilde{k}} \tag{7}$$

where G_k represents the generation of turbulent kinetic energy due to the mean velocity gradients. In a manner consistent with the Boussinesq hypothesis, G_k is calculated by Eq. (8). The term Y_k represents the dissipation of turbulent kinetic energy and is calculated by Eq. (9). Parameters $C_{1\varepsilon} = 1.44$, $C_{2\varepsilon} = 1.92$, $\sigma_k = 1.0$ and $\sigma_\varepsilon = 1.3$ are the constants (Ansys Inc, 2012).

$$G_k = \mu_t |\tilde{S}|^2, \ |\tilde{S}| = \sqrt{2\tilde{S}_{ij}\tilde{S}_{ij}} \tag{8}$$

$$Y_k = -\frac{\rho\tilde{k}^{\frac{3}{2}}}{l} \tag{9}$$

where l is the turbulence length scale. In the DDES model, a mixed turbulence length scale is used and given by

$$l = l_{RANS} - f_d max(0, l_{RANS} - l_{LES}) \tag{10}$$

where l_{RANS} and l_{LES} are the turbulence length scales of the RANS and LES models, respectively. f_d is a control function to select the regions applying the RANS and LES models. $f_d = 0$ represents that the realizable $k-\varepsilon$ model is used, while $f_d = 1$ represents that the LES model is applied. l_{RANS}, l_{LES} and f_d are expressed as

$$l_{RANS} = \frac{\tilde{k}^{\frac{3}{2}}}{\tilde{\varepsilon}} \tag{11}$$

$$l_{LES} = C_{des}\Delta_{max} \tag{12}$$

$$f_d = 1 - tanh\left[(A_1\gamma_d)^{A_2}\right] \tag{13}$$

where the constant $C_{des} = 0.032$ shown by Oka and Ishihara (2009) is adopted and $\Delta_{max} = \max(\Delta x, \Delta y, \Delta z)$ is used as described in Fluent Theory Guide (Ansys Inc, 2012).

$$\gamma_d = \frac{\upsilon_t + \upsilon}{\kappa^2 d^2 \sqrt{U_{ij} U_{ij}}}, \quad U_{ij} = \frac{\partial \tilde{u}_i}{\partial x_j} \tag{14}$$

where υ_t is the kinematic eddy viscosity, υ is the molecular viscosity, $\kappa = 0.41$ is the von Kaman constant, d is the distance to the closest wall and U_{ij} is the velocity gradient. In Fluent Theory Guide (Ansys Inc, 2012), $A_1 = 20$ proposed by Gritskevich et al. (2012) and $A_2 = 3$ are used for the realizable $k-\varepsilon$ and SST $k-\varepsilon$ based DDES models, while $A_1 = 8$ proposed by Spalart et al. (2006) and $A_2 = 3$ are used for the Spalart-Allmaras based DDES model. However, as mentioned by Ishihara and Qi (2019), the original DDES models were unable to well predict the separation flows with strongly organized motions behind a 3D smooth hill in the thick turbulent boundary layer, since the region applying RANS model was excessively high. In this study, the MDDES model proposed by Ishihara and Qi (2019) is used, in which a piecewise function of A_1 to limit the application of RANS model in the region below the surface layer height $h_{sl} = 1m$ at full scale. As shown in the following function, $A_1 = 0.2$ is used when the distance to the closest wall d is larger than h_{sl}, and the default value of $A_1 = 20$ is used if the distance d is smaller than h_{sl}.

$$A_1 = \begin{cases} 20, & d < h_s \\ 0.2, & d \geq h_s \end{cases} \tag{15}$$

2.2. Canopy model and wind turbine model

The generalized canopy model derived by Enoki and Ishihara (2012) and validated for trees and buildings by Qi and Ishihara (2018) is applied in this study to model the surface roughness covering the complex terrain, and the fluid force introduced in the momentum equations is shown as:

$$f_{\tilde{u},i} = -\frac{F_{\tilde{u},i}}{V_{grid}} = -\frac{1}{2}\rho C_f \frac{\gamma_0}{l_0} |\tilde{u}| \tilde{u}_i \tag{16}$$

where, $f_{\tilde{u},i}$ is the fluid force in the volume of grid, V_{grid}. $|\tilde{u}|$ is the absolute value of mean wind speed per unit volume, C_f is the equivalent drag coefficient, l_0 is defined as the representative length scale of obstacles and γ_0 is the packing density. $C_f = 0.4$, $\gamma_0 = 0.001$ and $l_0 = 0.01m$ are used for the forest canopy following the suggested value derived by Enoki and Ishihara (2012).

The utility-scale wind turbine in the Tomamae wind farm is adopted to study the wake over complex terrain. In the numerical wake simulation, the effect of the rotor induced forces on the flow is parameterized by using an actuator disk model with rotation (ADM-R), in which the lift and drag forces are calculated based on the blade element theory (Burton et al., 2011) and then unevenly distributed on the actuator disk. Fig. 1(a) shows the schematic of ADM-R model, where x is streamwise direction aligned with the incoming wind speed U_0. The azimuthal angle Φ shows the position of the blade in the tangential direction and it is 0 at the top position. The relation between wind velocity and forces acting on a blade element of length dr located at the radius r is shown in Fig. 1(b), where n and t denote the axial and tangential directions respectively, α is the angle of attack, β is the local pitch angle and ψ is the angle between the relative velocity and the rotor plane. dF_L and dF_D are the lift and drag forces acting on the blade element and given by:

$$dF_L = \frac{1}{2}\rho W^2 c C_L dr, \quad dF_D = \frac{1}{2}\rho W^2 c C_D dr \tag{17}$$

where c is the chord length, C_L and C_D are the lift and drag coefficients, respectively. W is the local relative velocity with respect to the blade element and is defined as:

$$W = \sqrt{U_n^2 + (\Omega r - U_t)^2} \tag{18}$$

where U_n and U_t are the axial and tangential velocities of the incident flow at the local blade element position. The resulting axial force dF_n and tangential force dF_t on the blade element can be expressed as:

$$dF_n = dF_L cos\psi + dF_D sin\psi \tag{19}$$

$$dF_t = dF_L sin\psi - dF_D cos\psi \tag{20}$$

The force per unit volume in each annular with an area of $\delta A = 2\pi r \delta r$ and a thickness of Δx is expressed by:

$$f_n = -\frac{B}{2\pi r}\frac{dF_n}{\Delta x \delta r} \tag{21}$$

$$f_t = -\frac{B}{2\pi r}\frac{dF_t}{\Delta x \delta r} \tag{22}$$

where B is the number of blades. The above obtained forces are then added as the source term in the numerical simulation to present the effects of the turbine rotor on the momentum.

2.3. Test site and measurement setup

In this study, a test site in the Tomamae wind farm, located in Hokkaido facing the Japan Sea, is considered. The prominent topographic feature of this site is a steep escarpment along the west coast as shown in

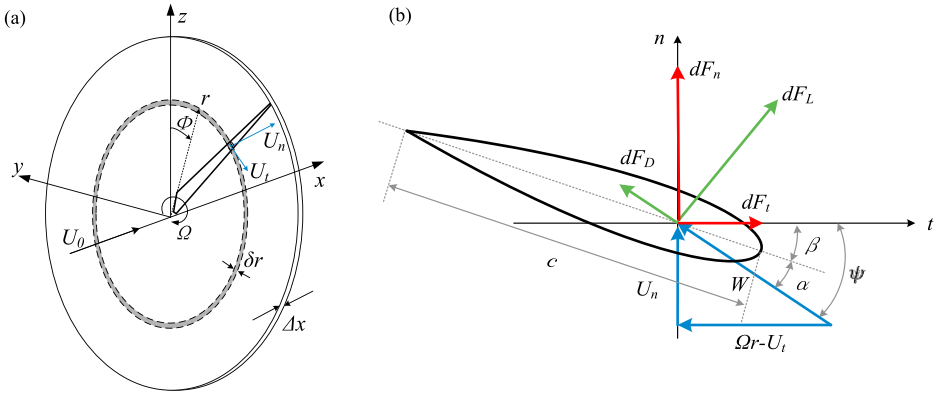

Fig. 1. Schematic of the ADM-R model for the turbine rotor: (a) axis system for a rotor and rotating element, (b) velocities and forces acting on a cross-sectional blade element.

Fig. 2. In addition, the east onshore site is mainly characterized by the ranch, farmland, grass, and nearby buildings and forests, which adds to the complexity of the land surface roughness. Comprehensive measurement campaigns were carried out successively in the Tomamae wind farm, including a ground-based vertical profile LIDAR from November 2015 to January 2016. The statistical data in every 10 min were recorded in the above measurement system. In this campaign, a Bonus B54/1000 1 MW wind turbine in the Tomamae wind farm is considered to study the wakes in complex terrain. The Bonus B54/1000 is an active stall-regulated turbine with a rotor diameter of D = 54.2 m and a hub height of H = 45.0 m.

2.4. Numerical setup

As shown in Fig. 3, the numerical wind tunnel is built by the dimensions of 18 km × 18 km × 2 km (streamwise direction, spanwise direction and vertical direction) with a scale of 1:2000. The height of domain is determined by limiting the blockage ratio to a specified value. 5% is often considered to be an acceptable limit of blockage ratio for a wind tunnel experiment (Fujino et al., 2012). Considering the average elevation in the site is lower than 100 m, 2 km is adopted as the calculation domain height. In the inflow generation zone, roughness blocks are placed 7 km upstream from the origin, following the experiment setup by Yamaguchi et al. (2003), where the neutrally stratified atmospheric boundary layer in the ocean side was simulated with the mean velocity profile following the power law of $\alpha = 0.1$. For the land side, the boundary layer would be automatically developed through the surrounding terrain and vegetations within the considered region as performed by Liu et al. (2016). The location of LIDAR is set as the origin of the computational domain for wind flow and wake flow simulation cases for WT03. The origin is then moved to No. 4 wind turbine (WT04), which is close to the escarpment edge as shown in Fig. 3 (b), to investigate the escarpment effects on the wake flow of WT04.

The topography model with a scale of 1:2000 and a radius R = 4 km is generated based on the digital elevation model (DEM), as shown in Fig. 3 (a). The DEM database used in this research is provided by the Geospatial Information Authority of Japan (2018) in raster format, which describes the topography in whole Japan with an available minimum resolution of 10 m × 10 m. The outer ring with width of 1 km is used to smooth the surrounding terrain. Since the buildings and forest are dominant surface roughness conditions and strongly affect above flow fields, the canopy model described in section 2.2 is applied. The distribution of the vegetation and buildings are obtained from the database provided by the Ministry of Land, Infrastructure, Transport and Tourism (2014) and then locally modified based on the Google map. The average height of forest is set as 13.3m for the canopy layers with the parameters determined based on the procedure proposed by Enoki and Ishihara (2012).

For the sake of reducing calculation cost as well as keeping prediction accuracy, a hybrid grid system is designed as shown in Fig. 4. As shown by Wu and Porté-Agel (2011) for LES type framework, around 20 grid points covering the rotor diameter are necessary to be capable of accurately reproducing wind-turbine wake characteristics (including mean

Fig. 2. Test site in the Tomamae wind farm: (a) location of Tomamae; (b) aerial picture of wind farm; (c) wind turbine and its dimensions; (d) layout of the wind farm and measurement where the white open circles denote the location of each wind turbine and the red square indicates the position of LiDAR. (For interpretation of the references to colour in this figure legend, the reader is referred to the Web version of this article.)

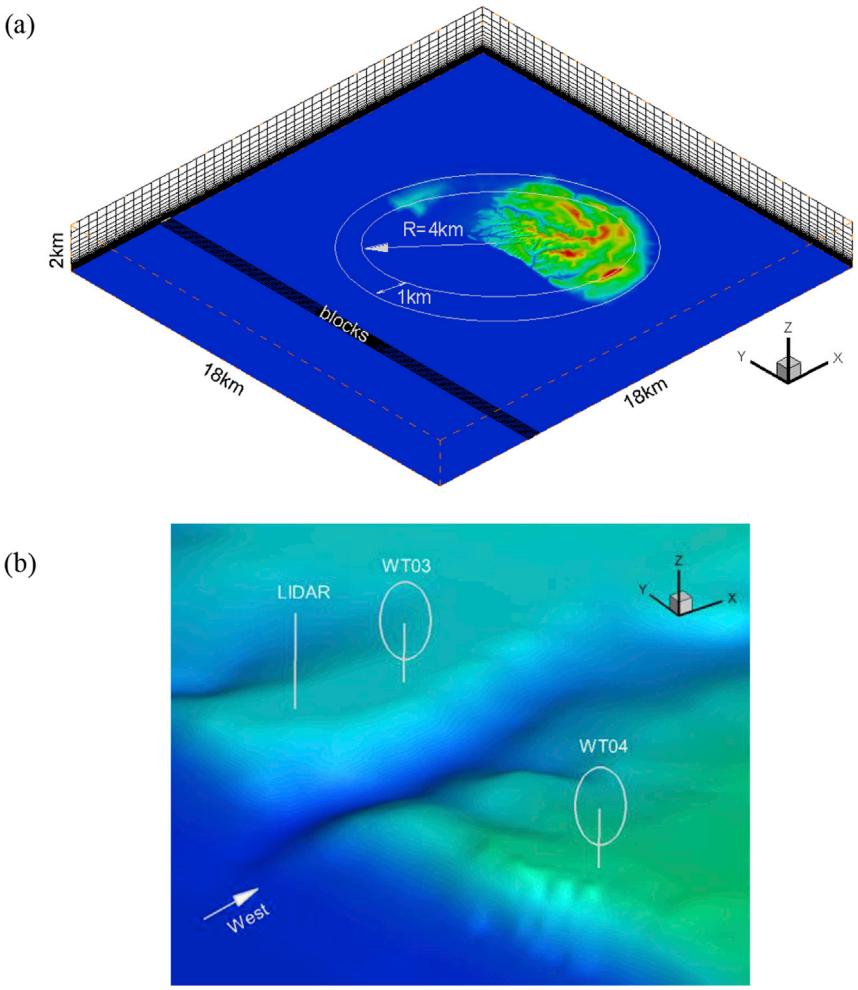

Fig. 3. Configuration of the computational domain: (a) global view of the domain; (b) local view of the terrain near the WT03, WT04, and LiDAR.

velocity, turbulence intensity and turbulence fluxes). Therefore, in the turbine wake zone as shown in Fig. 4 (d), a resolution of 2m in horizontal direction is used to capture the detailed turbulence features for the turbine wake flow over complex terrain. A target zone as shown in Fig. 4 (b) is a square centered at the origin with side length of 2 km to consider the effects from the closely surrounding terrain and vegetation, in which three grid resolution levels δx of 16 m, 8 m, and 4 m are tested. The root mean squared errors (RMSE) of the normalized wind speed predicted by these three grid levels are summarized in Fig. 5, where only the wind directions from the land side without turbine wake effects are considered. It is found that for high elevation of $h = 100$ m, all the three grid resolutions provide almost same accuracy, while for the elevation around turbine hub height, i.e. $h = 40$ m, grid resolution of 8 m is enough for providing grid independent results and thus is adopted in the target zone. Relative coarse grid resolution is used in the buffer zone as shown in Fig. 4 (a). An additional upstream buffer zone is appended in front of roughness blocks to avoid perturbations from the inlet condition. The σ grid system is applied to modify the vertical coordinate of grid nodes above the topography, which means keeping the ratio of the vertical size of adjacent grids unchanged. The vertical grid size of the first layer is set as 0.4 m at full scale with an expansion factor of 1.15. As illustrated in Fig. 6, numerical simulations for different wind direction are performed using the same grid system, as implemented like the turn table in a wind tunnel, which means the coordinated of the terrain are rotated when the wind direction is changed.

Finite volume method is employed in this study and the simulations are performed with ANSYS Fluent. The central difference scheme is applied for the interpolation of velocities and second order upwind scheme is used for the turbulent kinetic energy and dissipation rate. SIMPLE (semi-implicit pressure linked equations) algorithm is employed for solving the discretized equations. A second-order implicit scheme is applied to approximate the time derivatives for the unsteady term (Ferziger and Perić, 2002). The non-dimensional time step size is set as $\Delta tU/H = 0.044$, where H is the turbine hub height and U is the inlet wind speed. The Courant-Friedrichs-Lewy number (Courant et al., 1928) expressed as $C = \Delta t \sum \tilde{u}_i / \Delta x_i$ (i=1,2,3), where $\tilde{u}_i$ is the velocity and Δx_i is the grid size, is monitored to ensure $C_{\max} < 1.0$ in the whole computational domain. Additionally, the residual values of six variables (i.e. continuity, u, v, w, k and ε) are also monitored during the calculation process. For each time step, the solution is deemed to be converged when these residual values are below than 10e-4. Boundary conditions used in the numerical simulations are summarized in Table 1. A stress-free condition ($\partial u/\partial n = 0$, $\partial v/\partial n = 0$, $w = 0$) is used at the top of the domain and a symmetry condition ($\partial u/\partial n = 0$, $\partial w/\partial n = 0$, $v = 0$) at the two sides. Uniform flow with a speed of 10 m/s is set at the inlet ($p = 0$, $u = 10$ m/s, $v = 0$, $w = 0$, $k = 0.001\ m^2/s^2$, $\varepsilon = 0.001\ m^2/s^3$). At the end of the tunnel, the outflow condition is applied ($\partial p/\partial n = 0$, $\partial u/\partial n = 0$, $\partial v/\partial n = 0$, $\partial w/\partial n = 0$).

The wall-stress boundary condition is imposed at the ground surface with the roughness height $z_0 = 0.0002$m for ocean area and $z_0 = 0.03$m for land area and the ground surface under the canopies, such as forest and buildings, respectively. For the wall-adjacent cells, the wall shear stresses are obtained based on the log law of wall with the modification for roughness as follows:

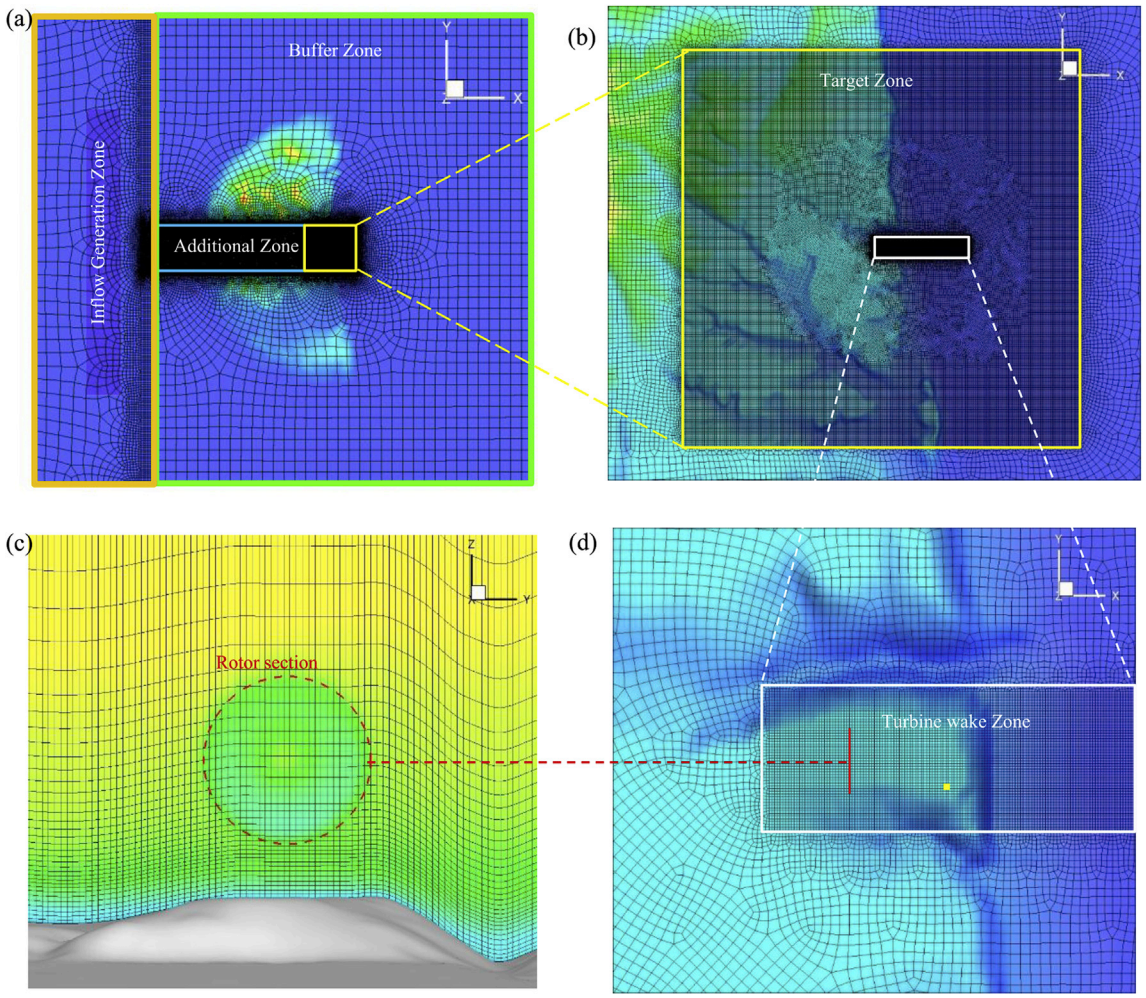

Fig. 4. Hybrid grid system of computational domain: (a) whole domain; (b) target zone; (c) rotor section; (d) wake zone.

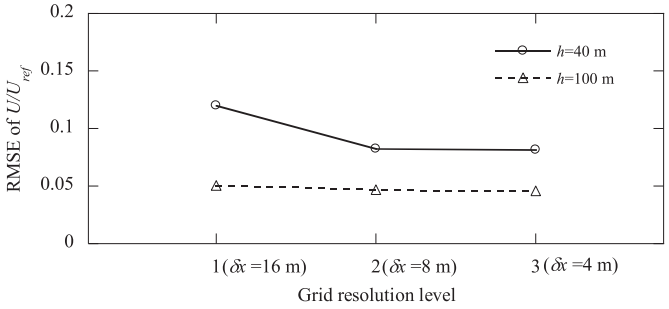

Fig. 5. RMSE of the normalized mean wind speed U/U_{ref} versus horizontal grid resolution level in the target zone. U_{ref} is the mean wind speed at the height of $h = 120$ m. The Solid line with open circles represents result at the height of $h = 40$ m, and the dashed line with triangles denotes results at the height of $h = 100$ m.

$$\frac{\overline{u}}{u_*} = \frac{1}{\kappa}\ln\left(E\frac{\rho u_* z}{\mu}\right) - \Delta B \tag{23}$$

where $\overline{u}$ is the resolved velocity tangential to the wall, z is the distance between the center of the cell and the wall, $u_* = C_\mu^{1/4}k^{1/2}$ is the friction velocity, and the constant E is 9.793. ΔB accounts for the displacement caused by the rough wall and is 0 for the smooth wall. The logarithmic law as shown in the following equation is widely used as the boundary condition for neutrally stratified atmospheric boundary layers (Blocken et al., 2007; Grimmond et al., 1999; Xian et al., 2002).

$$\frac{\overline{u}}{u_*} = \frac{1}{\kappa}\ln\left(\frac{z}{z_0}\right) \tag{24}$$

where z_0 is the aerodynamic roughness length and is defined as the height above the ground at which the mean velocity is 0. ΔB can be calculated by comparing Eq. (23) and Eq. (24)

$$\Delta B = \frac{1}{\kappa}\ln\left(E\frac{\rho u_* z_0}{\mu}\right) \tag{25}$$

It should be noted that, In ANSYS Fluent, the law of the wall for mean velocity is based on the non-dimensional distance from the wall, $y^* = \rho u_* z/\mu$, rather than $y^+ = \rho u_\tau z/\mu$, where $u_\tau = (\tau_w/\rho)^{1/2}$ with τ_w defined as the wall shear stress. In this study, the smallest y^* values achieved in the simulations are kept in the order of $y^* \sim 15$, which meets the requirement that the above described logarithmic law is employed only when $y^* > 11.225$ (Ansys Inc, 2012).

2.5. Validation

Firstly, the atmosphere boundary layer without terrain and wind turbine is generated by the roughness blocks to provide the inlet flow condition for further simulations. The vertical profiles at the location of 3.5 km downwind the roughness blocks are presented in Fig. 7, where measurement data obtained from the experiment by Yamaguchi et al. (2003) are also plotted for comparison. Note that the mean wind speed U

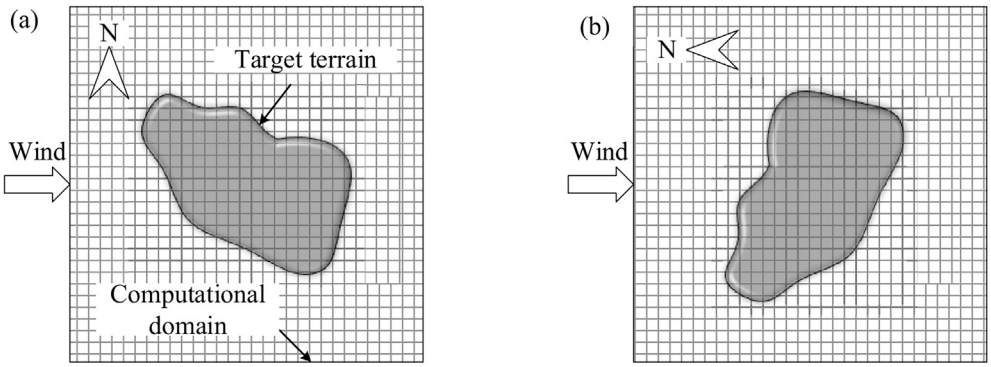

Fig. 6. Schematic of numerical simulation for terrain under different direction: example of (a)West wind and (b) North wind.

Table 1
Boundary conditions in simulations.

Boundary	Setting
Inlet	Velocity inlet
Outlet	Outflow
Side	Symmetry
Top	Symmetry
Bottom	Logarithmic law

are normalized by the reference value U_{ref} at the height of 150m, and the turbulence intensity is defined as the ratio of standard deviation of fluctuating wind speed σ_u to mean wind speed U at each height. It can be observed that the numerical simulated vertical profiles show good agreement with the experiment data, which implies that the generated inflow satisfy with the atmospheric boundary layer in the ocean side with the mean velocity profile following the power law of $\alpha = 0.1$.

To verify the accuracy of the MDDES model and the boundary conditions described above, the wind flow in the boundary layer without turbines is predicted and compared with the measurements. As shown in Fig. 8, in the West, North-East and South directions LiDAR are not affected by the wind turbine wakes. The vertical profiles of the mean wind speed at the location of LiDAR under these three specific wind directions are shown in Fig. 9. The mean velocity is normalized by the referred value U_{ref} measured by LiDAR at the height of 120m. The error bars in the measurements show the standard deviations of the averaged values. Obvious differences of the gradient of the velocity profiles can be found in those directions since the terrain and surface roughness vary with the wind directions. In the West direction, wind is from the ocean side and there is a speed up at the low elevation over the escarpment. The numerical results show favourably good agreement with the measurements without the effect of wind turbine wake.

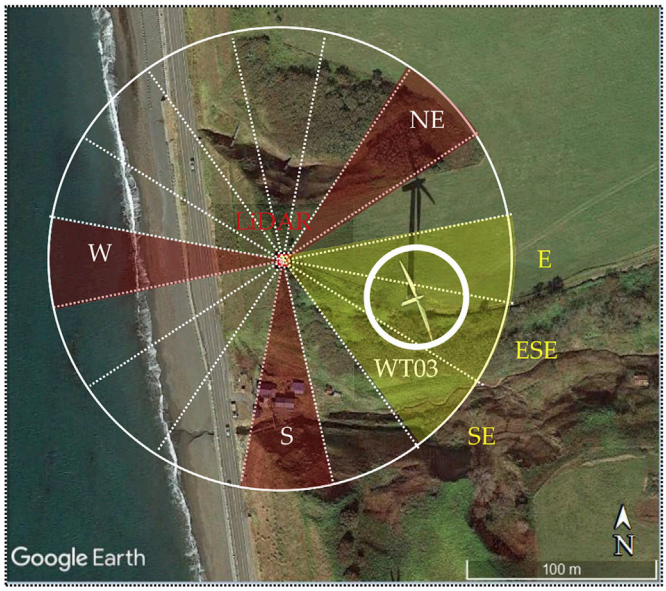

Fig. 8. Schematic of wind flow simulation cases for terrain in West (W), North-East (NE), and South (S) directions and wake flow simulation cases for WT03 in East (E), East-South-East (ESE), South-East (SE) wind directions.

As shown in Fig. 8, the LiDAR is located with the distance of 1.4D from the No.3 wind turbine (WT03), it is significantly affected by the wind turbine wake. Numerical simulations of the turbulent wake flow over the terrain are performed for WT03 in three representative wind

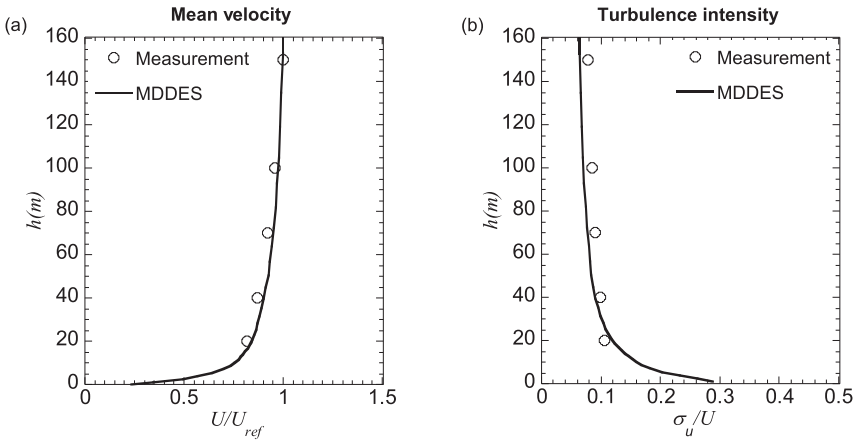

Fig. 7. Vertical profiles of generated atmosphere boundary layer over flat terrain: (a) normalized mean velocity and (b) turbulence intensity.

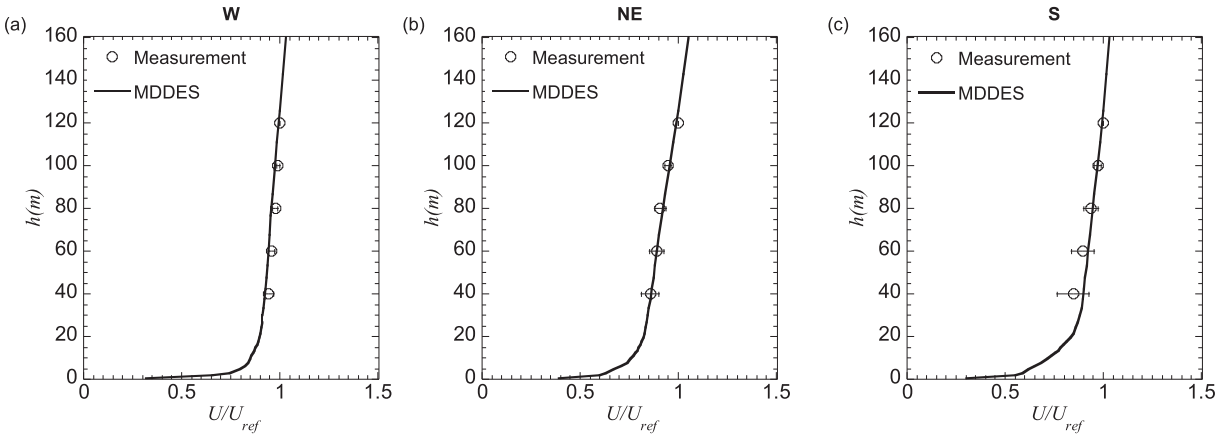

Fig. 9. Comparison between predicted and measured wind flows at the location of LiDAR: (a)West wind direction, (b) North-East wind direction, (c)South wind direction.

directions of East, East-South-East and South-East and are presented in Fig. 10. The wind turbine is always kept normal to the onset flow for each case. Since the wake behavior are directly related with the turbine operation condition, the plotted mean wind speeds by LiDAR are bin averaged values with the criteria of $U_{SCADA} \pm 0.5$m/s, where the U_{SCADA} is the mean wind speed measured by the SCADA of WT03. The reference mean wind speeds U_{ref} at the height of 120m are used for normalization of velocity. The error bars in the measurements show the standard deviations of the averaged values. A significant deceleration of the wind flow is observed in the turbine rotor area because of the extracted energy by the wind turbine. As shown in Fig. 11, in E and SE directions, the positions of LiDAR are closely located at the edge of wind turbine wake region, while in ESE direction LiDAR is almost in the center of the wake, resulting in wider wake region and stronger velocity deficit compared with those in E and SE directions. It is found that the velocity deficits in these three wind directions are well reproduced by the numerical model. To provide a wider range of results for validation, the distribution of wind speed under each wind direction from measurement and simulations are presented in Fig. 12, where open circles and squares represent LiDAR data at height of 40 m and 100 m, respectively, while the corresponding results obtained from numerical simulations are plotted by solid and dashed lines for comparison. Generally, simulated results also match well with the measured data. Note that the height of 100 m is higher than the top tip side of turbine and thus the wind speed is not affected by turbine wakes. For the results at height of 40m, an obvious concave can be observed between ENE and SSE due to the wake effects from WT03, which is consistent with the results presented in Fig. 10.

3. A hybrid framework for wake modelling over complex terrain

A hybrid framework for wind turbine wake modelling over complex terrain is presented and verified in this section. The formulation of the hybrid framework, which involves numerical simulation and analytical wake model, is illustrated in section 3.1. In section 3.2, the wake flow behaviours over escarpments with different elevations are systematically investigated by using the numerical simulation. In section 3.3 the proposed framework is verified by comparison with the numerical results presented in section 3.2.

3.1. Formulation of the hybrid framework

In a real wind farm, complex terrain mainly induces the variation of wind speed, turbulence intensity, and wind direction. In order to reduce the computational cost of wind turbine wakes while retaining a comparable accuracy with the full CFD simulation, a hybrid framework is utilized for wake effects evaluation in the real wind farm. In this framework, the effects of local terrain and surface roughness on the wind speed, wind direction and turbulence are taken into account by the numerical simulation as implemented by Misu and Ishihara (2018), while the wind turbine wakes are represented by a new Gaussian-based analytical wake

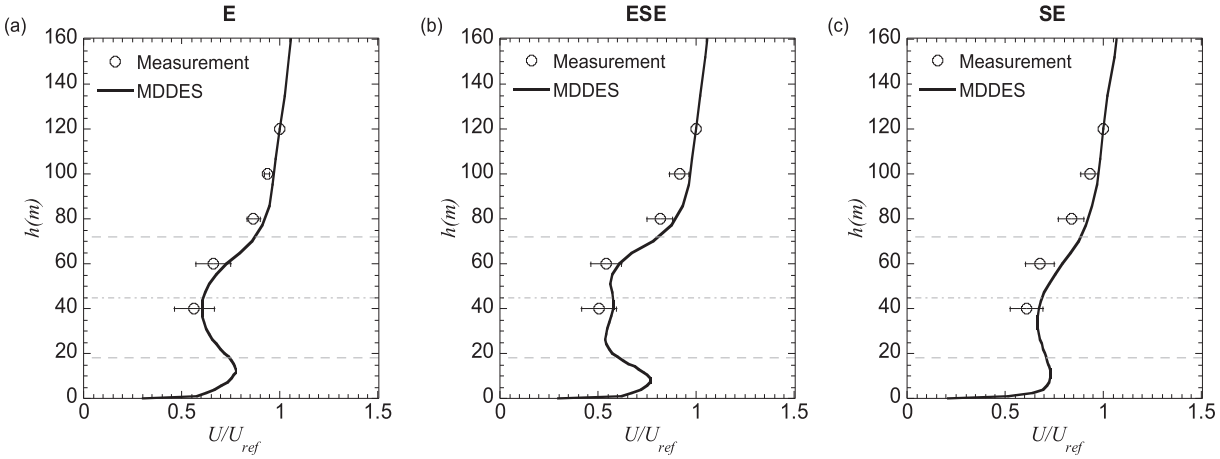

Fig. 10. Comparison between predicted and measured wind turbine wake flows at the location of LiDAR for normalized mean streamwise velocity: (a) East wind direction, (b) East-South-East wind direction, (c) South-East wind direction. The two dashed lines mark the turbine bottom and top tips, dot-dashed lines show the hub height position. The averaged wind speeds U_{SCADA} at the hub height are 10 m/s, 7 m/s, and 7 m/s for E, ESE, and SE.

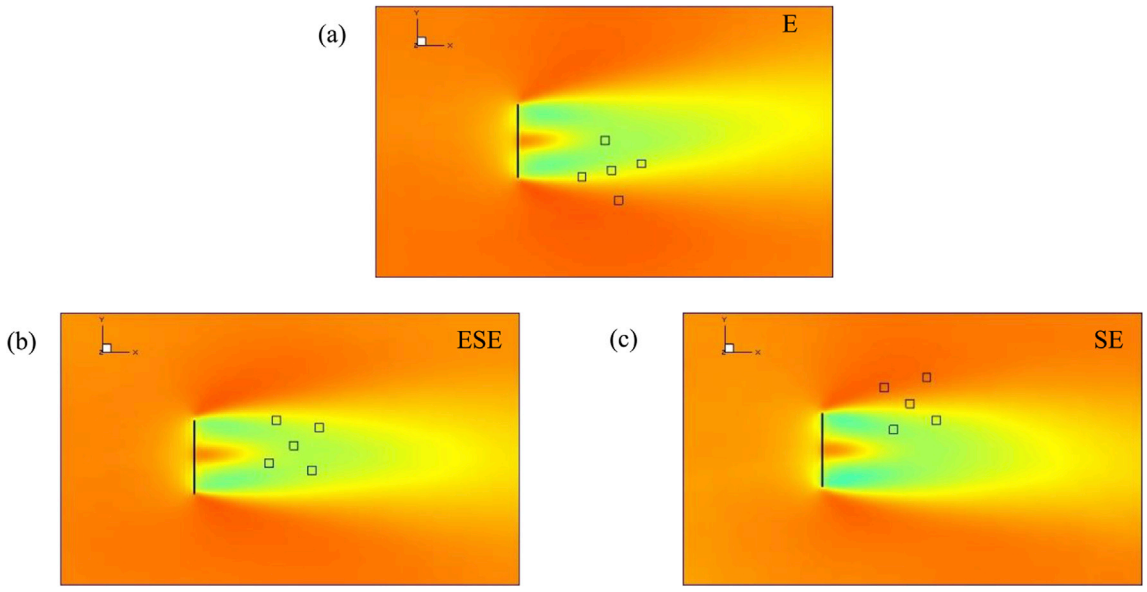

Fig. 11. Local view of mean streamwise velocity contours in horizontal $x-y$ plane at the height of 40 m from ground: (a), (b) and (c) are for E, ESE and SE wind directions, respectively. The open squares mark the five beams' positions of LiDAR and the solid lines denote the turbine rotor plane. The vertical profiles in the numerical simulation are obtained using the same approach as the real LiDAR, i.e. Doppler Beam Swinging (DBS) mode with five beams in one scanning circle.

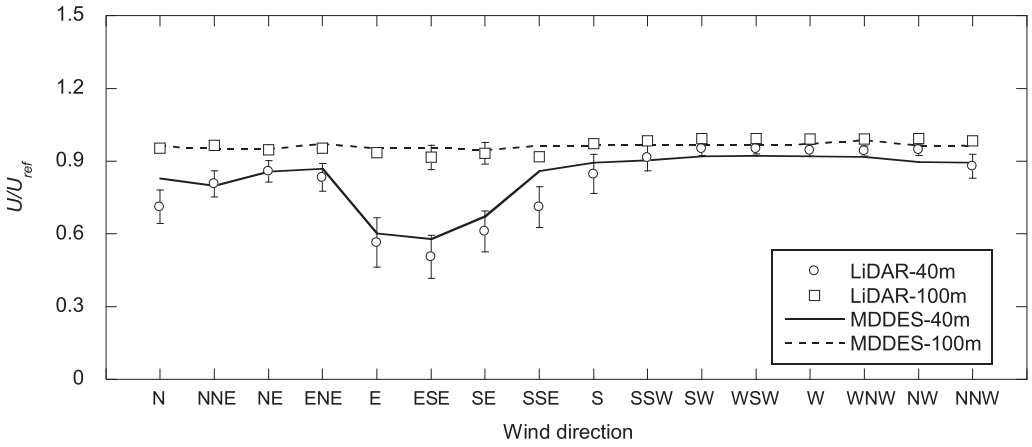

Fig. 12. Distribution of normalized mean streamwise velocity at selected heights of 40 m and 100 m under different wind directions.

model which can consider the terrain induced yaw misalignment effects (Ishihara and Qian, 2018; Qian and Ishihara, 2018). The inclination angle effects are analogously applied to this model as the yaw angle. It should be noted that the wind farm layout optimization and the control-based power production maximization are an iterative process, in which turbine wake effects are required to be evaluated for a large number of iterations. In the current hybrid framework, only the initial turbulent flow field due to the complex terrain is provided by the CFD simulation, while turbine wake effects under different wind speeds and wind directions are evaluated by the analytical wake model in each iteration to determine the optimized turbine positions and control strategies. Therefore, the current hybrid framework is extremely efficient than the full CFD simulation for the wind farm layout optimization and control-based power production maximization over the complex terrain.

The detailed procedures to set up the hybrid framework are illustrated in Fig. 13. Firstly, based on the digital elevation model (DEM) (Geospatial Information Authority of Japan, 2018) and the surface roughness database (SRD) (Ministry of Land, Infrastructure, Transport and Tourism, 2014), numerical simulations by using the MDDES model without turbines are performed to provide the wind field information including the wind speed U_0, local wind direction angle γ_y, γ_z and standard deviation of streamwise velocity σ_{u0} without the wind turbine wake effects. DEM provides the topographic elevation data in raster format with an available resolution of meters, and it is used to represent the terrain effects on the local wind field. SRD supplies the land use information in raster format and also the shape files of the vegetation and buildings in vector format. SRD is used to express the effects of ground surface roughness and canopies such as vegetation and buildings on the ABL development in the local sites. Subsequently, the numerical simulated local wind field information is extracted as the input for the new Gaussian-based analytical wake model to calculate the turbine induced wake deficit ΔU and added turbulence $\Delta\sigma_u$ as follows:

$$\Delta U(x,r)/U_h = F\left(C_T, I_a, x/D, \gamma_y, \gamma_z\right)\phi(r/\sigma) \tag{26}$$

$$\Delta\sigma_u(x,r)/U_h = G\left(C_T, I_a, x/D, \gamma_y, \gamma_z\right)\varphi(r/\sigma) \tag{27}$$

$$r = \sqrt{(y-y_d)^2 + (z-H_{hub}-z_d)^2} \tag{28}$$

where F and ϕ are the streamwise and spanwise function for velocity deficit, G and φ denote the streamwise and spanwise function for

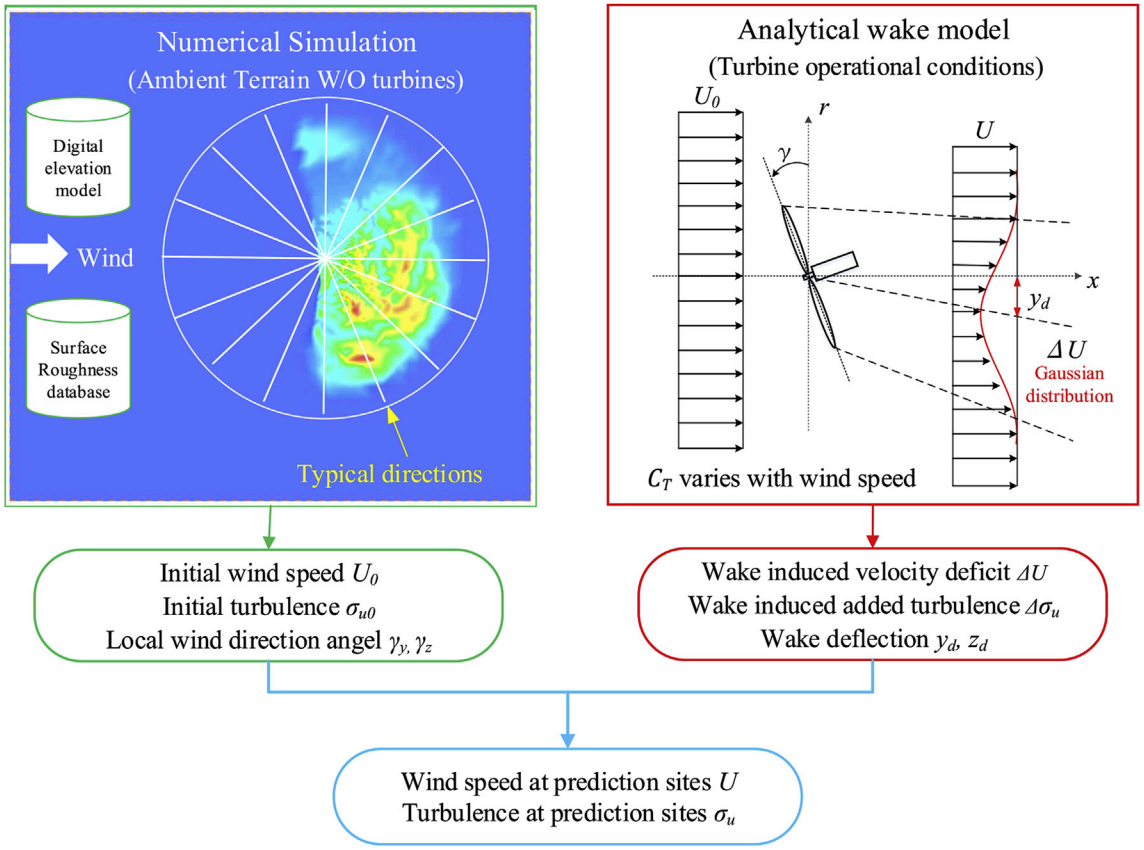

Fig. 13. Schematic of the hybrid framework for wind turbine wake flow prediction over complex terrain.

added turbulence, U_h is the incoming wind speed at the hub height of the upstream wind turbine, C_T is the thrust coefficient, I_a is the ambient turbulence intensity at the hub height, x/D is the streamwise distance from the turbine normalized by rotor diameter, H_{hub} is the hub height, r is the distance from the wake center in the radial direction, σ is treated as the wake representative width, γ_y and γ_z represent the local yaw and inclination angles respect to the wind turbine, y_d and z_d are the wake deflection in the horizontal and vertical directions. All the wake model parameters are determined as the function of I_a and C_T and the detailed expressions can be found in Ishihara and Qian (2018) and Qian and Ishihara (2018). Finally, by the superposition of analytical model calculated wake effects and CFD resolved wind field without the wind turbine wake effects, the wind fields considering the wake effects at the prediction sites are obtained as shown in Eq. (29) and Eq. (30).

$$U = U_0 - \Delta U \tag{29}$$

$$\sigma_u = \sqrt{\sigma_{u0}^2 + \Delta\sigma_u^2} \tag{30}$$

3.2. Escarpment induced terrain effects on the wind turbine wake

The escarpment is one of the most representative terrain in the coastal region of Japan and is used to investigate terrain effects on the wind turbine wakes in this study. As shown in Fig. 3 (b), the No. 4 wind turbine (WT04), located close to the edge of the escarpment, is chosen for the numerical study with the incoming wind direction of West. Two different terrain heights are considered with the scale ratios of $H_{hill}/H_{hub} = 0.9$ for the low escarpment case and $H_{hill}/H_{hub} = 3.6$ for the high escarpment case, respectively, where H_{hill} is the local elevation of terrain at the turbine site. The original slope of the terrain is kept for these two cases for the comparison. Firstly, the numerical simulations are carried out without the turbine to examine the wind flow features over the escarpments. It is observed that the wind direction changes not only in the vertical direction but also in the horizontal direction as the edge of the escarpment is not regularly perpendicular to the wind direction. Fig. 14 presents the variation of the wind direction changes at the hub height, where $x/D = 0$ represent the location of wind turbine. The terrain induced inclination and yaw angles are larger over the higher escarpment. The inclination angle decreases rapidly in the downwind regions to an almost constant value around 1°, while the yaw angle decreases slowly.

The wind turbine wakes over the escarpments are simulated based on the operational condition of constant rotational speed of 21 rpm (round per minute). Fig. 15 illustrates the simulated wake flows over the two escarpments with different heights, where the contours of the mean velocity are normalized by U_h, the wind speed at the hub height without the wind turbine. In the vertical direction, the wakes are lifted up in the near wake region, but not distinctly in the far wake region as shown in Fig. 15 (a) and (b). This is due to the fact that the terrain induced inclination angles are quite small downwind the turbine. In the horizontal direction, an obvious wake deflection is observed for the high escarpment case, while there is no significant lateral displacement of the wake for the low escarpment case since the yaw misalignment angle is much smaller than that over the high escarpment as shown in Fig. 15 (c) and (d). The main terrain effects discussed in this paper are the escarpment induced yaw and inclination angles on the turbine, which result in the wake deflection in horizontal and vertical. For the low escarpment case, one can clearly identify from Fig. 15 that the wake is almost not deflected as it behaves over the flat terrain. It is concluded that the terrain effects are negligible when the steep escarpment is lower than the turbine hub height, however, the steep escarpment with the elevation much higher than the hub height influences the wake behavior significantly.

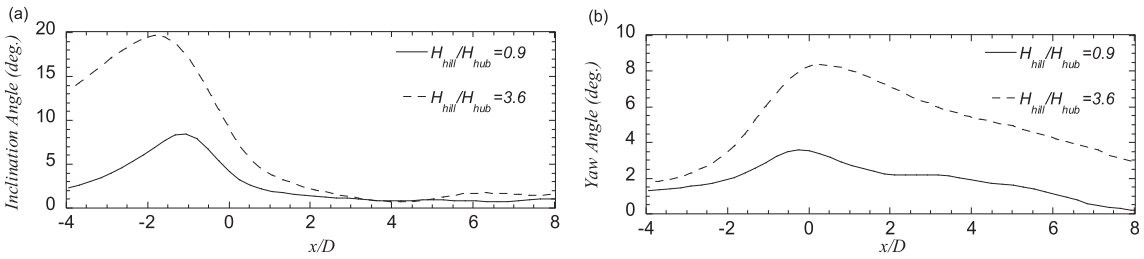

Fig. 14. Terrain induced wind direction changes at the hub height: (a)inclination angle in the vertical direction; (b) yaw angle in the horizontal direction.

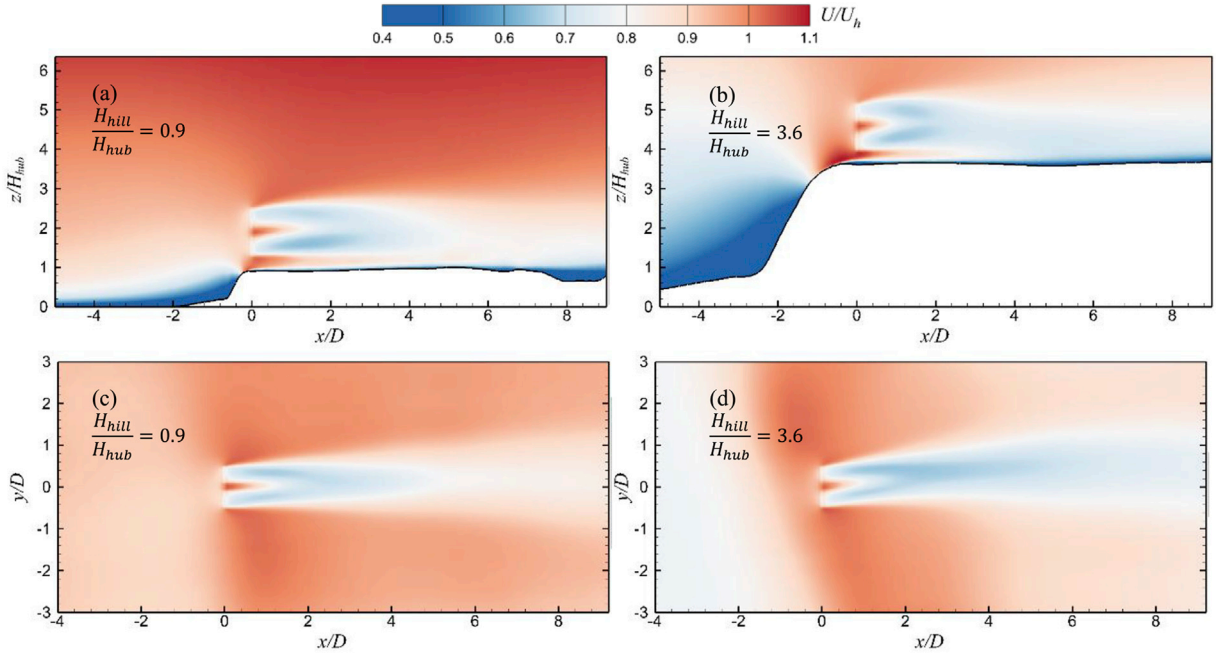

Fig. 15. Wind turbine wake flow over the escarpment: (a), (b) for x-z plane through the turbine rotor center; (c), (d) for x-y plane at the hub height.

3.3. Verification

In this section, the accuracy of the developed hybrid framework for wake modelling over the escarpments is examined by the full CFD simulations presented in section 3.2. The numerical simulation without the wind turbine provides the initial wind field, including wind speed, turbulence intensity, local yaw and inclination angle at the hub height, which is used as the input for the analytical wake model. Then the calculated velocity deficit and added turbulence intensity are superposed on the initial field without wind turbine wake effects and then compared with those from the full CFD simulation.

The vertical and horizontal profiles of the normalized mean velocity U/U_h and turbulence intensity σ_u/U_h at the selected downwind locations of $x = 2.6D$, $4D$, $6D$, $8D$ are plotted in Figs 16 and 17, respectively. The minimum distance between turbines is around $2.6D$ in the Tomamae wind farm, thus the comparison of profiles starts from $x = 2.6D$. The x-axis denotes the distance from the wind turbine normalized by the rotor diameter D. The distance of $2D$ corresponds to a unit scale of normalized mean velocity U/U_h in Fig. 16 (a, c) and Fig. 17 (a, c), while in Fig. 16 (b, d) and Fig. 17 (b, d), it corresponds to a scale of turbulence intensity σ/U_h with the value of 0.3. Open circles denote the MDDES results obtained from a full CFD simulation including the ADM-R for turbine, and red solid lines represent the wake model values from the proposed hybrid approach, where the turbine wakes are predicted by the new Gaussian analytical wake model with the wake deflection considering the terrain induced yaw and inclination effects. The values predicted by the wake model without considering the wake deflection are also plotted by black dashed lines for comparison, where the escarpment induced yaw and inclination angles are not inputted in the wake model calculation.

It can be seen that, for the wake over escarpment with low elevation case, both the wake models with and without the wake deflection give favourable agreement with the full CFD simulated results by MDDES. While for the high escarpment case, the wake model with the wake deflection considering the terrain induced inclination and yaw angle effects gives more accurate prediction both in the horizontal and vertical directions. It is noted that obvious enhancements of turbulence occur in the upper half of the wake region as well as near the two side-tip positions in the horizontal directions, which are related to the strong shear layers in the wake boundary region. Since the turbine wake is deflected over the high escarpment, the variation of turbulence is also correspondingly deflected in the horizontal and vertical direction and this phenomenon is well captured by the wake model with deflection especially at the locations of $x/D = 2.6$ and 4.

It should be noted here that, since the terrain induced yaw angle in the current case is smaller the yaw misalignment of 8° defined by IEC standard (IEC61400-1, 2019), the wind turbine is fixed aligned with the West direction in this study. In the current hybrid framework, the wake model is to consider the yaw misalignment effects induced by the terrain, if the wind direction changes with an angle larger than the specified angle for the yaw control, the wind turbine should be yawed aligned with the local wind direction.

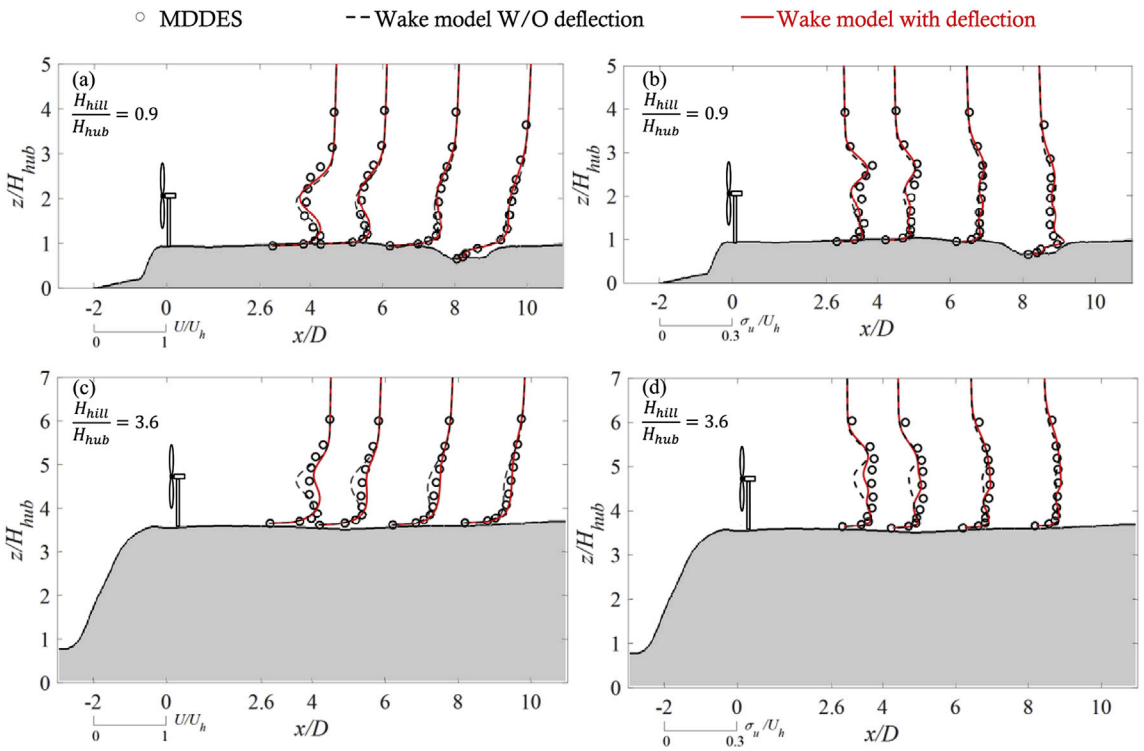

Fig. 16. Comparison of predicted vertical profiles of mean velocity and turbulence intensity in the plane of y = 0 through the rotor center: (a) and (b) for the wake over low elevation escarpment, (c) and (d) for the wake over high elevation escarpment.

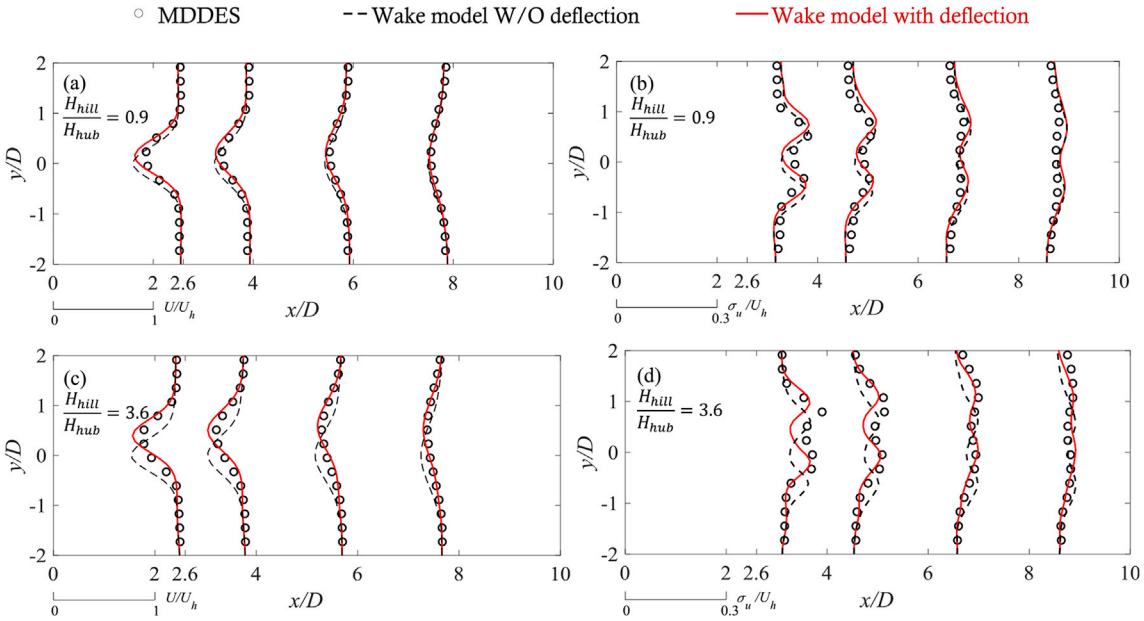

Fig. 17. Comparison of predicted horizontal profiles of mean velocity and turbulence intensity in the plane of x-y at the hub height: (a) and (b) for the wake over low elevation escarpment, (c) and (d) for the wake over high elevation escarpment.

4. Conclusion

In this study, numerical simulations on the wind turbine wake flow over complex terrain are conducted by using the MDDES model and a hybrid framework is utilized for wake flow prediction over complex terrain. The numerical results are validated by measurement campaigns conducted in a real wind farm, and the hybrid framework is verified by the numerical simulation. Following conclusions are obtained:

(1) The predicted wind flow without and with wind turbine wake over the complex terrain based on a MDDES model show favourable agreement with the measurement data.
(2) The escarpment terrain effects on the wind flow and wind turbine wake are investigated by the MDDES model. The wind direction changes both in the vertical and horizontal direction with the inclination and yaw misalignment angle regard to the wind turbine on the escarpment with an irregular edge. The terrain effects on the wind turbine wakes are small when a steep escarpment is

lower than the turbine hub height. However, their influences on the wake behavior are significant when a steep escarpment is with the elevation several times of the hub height.

(3) A hybrid framework is utilized for wind turbine wake prediction over complex terrain, in which the effects of local terrain and surface roughness are taken into account by the numerical simulation, while the wind turbine wakes are represented by a new Gaussian-based analytical wake model considering the terrain induced yaw and inclination angle effects. The proposed framework is verified by the numerical simulations and shows good performance for prediction of wind turbine wakes over the escarpment.

Acknowledgements

This research was carried out as a part of the project funded by New Energy and Industrial Technology Development Organization (NEDO). The authors express their deepest gratitude to the concerned parties for their assistance during this study.

References

Ansys Inc, 2012. ANSYS Fluent Theory Guide. Canonsburg, PA.
Bechmann, A., Sørensen, N.N., 2010. Hybrid RANS/LES method for wind flow over complex terrain. Wind Energy 13, 36–50.
Berg, J., Troldborg, N., Sorensen, N.N., Patton, E.G., Sullivan, P.P., 2017. Large-Eddy Simulation of turbine wake in complex terrain. J. Phys. Conf. Ser. 854.
Blocken, B., Stathopoulos, T., Carmeliet, J., 2007. CFD simulation of the atmospheric boundary layer: wall function problems. Atmos. Environ. 41, 238–252.
Burton, T., Sharpe, D., Jenkins, N., Bossanyi, E., 2011. Wind Energy Handbook, second ed. Wiley.
Courant, R., Friedrichs, K., Lewy, H., 1928. Uber die partiellen Differenzengleichungen der mathematischen Physik. Math. Ann. 100, 32–74.
Crespo, A., Manuel, F., Grau, J.C., Hernández, J., 1993. Modelization of wind farms in complex terrain. Application to the Monteahumada wind farm. In: European Community Wind Energy Conference. Travemünde, pp. 440–443.
Daaou Nedjari, H., Guerri, O., Saighi, M., 2017. CFD wind turbines wake assessment in complex topography. Energy Convers. Manag. 138, 224–236.
Enoki, K., Ishihara, T., 2012. A generalized canopy model and its application to the prediction of urban wind climate. J. Japan Soc. Civ. Eng. 68, 28–47 (in Japanese).
Feng, J., Shen, W.Z., 2014. Wind farm layout optimization in complex terrain: a preliminary study on a Gaussian hill. J. Phys. Conf. Ser. 524, 012146.
Ferziger, J.H., Perić, M. (Milovan), 2002. Computational Methods for Fluid Dynamics. Springer.
Fujino, Y., Kimura, K., Tanaka, H., 2012. Wind Resistant Design of Bridges in Japan: Developments and Practices.
Geospatial Information Authority of Japan, 2018. http://www.gsi.go.jp/ENGLISH/index.html.
Grimmond, C.S.B., Oke, T.R., Grimmond, C.S.B., Oke, T.R., 1999. Aerodynamic properties of urban areas derived from analysis of surface form. J. Appl. Meteorol. 38, 1262–1292.
Gritskevich, M.S., Garbaruk, A.V., Schütze, J., Menter, F.R., 2012. Development of DDES and IDDES formulations for the k-ω shear stress transport model. Flow. Turbul. Combust. 88, 431–449.
Hyvärinen, A., Segalini, A., 2017. Qualitative analysis of wind-turbine wakes over hilly terrain. IOP Conf. Ser. J. Phys. Conf. Ser. 854, 12023.
IEC61400-1, 2019. Wind Turbines - Part 1: Design Requirements.
Ishihara, T., Qi, Y., 2019. Numerical study of turbulent flow fields over steep terrains by using a modified delayed detached eddy simulations. Boundary-Layer Meteorol. 170 (1), 45–68.
Ishihara, T., Qian, G.-W., 2018. A new Gaussian-based analytical wake model for wind turbines considering ambient turbulence intensities and thrust coefficient effects. J. Wind Eng. Ind. Aerodyn. 177, 275–292.
Ishihara, T., Yamaguchi, A., Fujino, Y., 2004. Development of a new wake model based on a wind tunnel experiment. Glob. Wind Power.
Jensen, N.O., 1983. A Note on Wind Generator Interaction, Risø-M-2411 Risø National Laboratory Roskilde.
Kuo, J., Rehman, D., Romero, D.A., Amon, C.H., 2018. A novel wake model for wind farm design on complex terrains. J. Wind Eng. Ind. Aerodyn. 174, 94–102.
Liu, Z., Ishihara, T., He, X., Niu, H., 2016. LES study on the turbulent flow fields over complex terrain covered by vegetation canopy. J. Wind Eng. Ind. Aerodyn. 155, 60–73.
Makridis, A., Chick, J., 2013. Validation of a CFD model of wind turbine wakes with terrain effects. J. Wind Eng. Ind. Aerodyn. 123, 12–29.
Migoya, E., Crespo, A., García, J., Moreno, F., Manuel, F., Jiménez, Á., Costa, A., 2007. Comparative study of the behavior of wind-turbines in a wind farm. Energy 32, 1871–1885.
Misu, Y., Ishihara, T., 2018. Prediction of frequency distribution of strong crosswind in a control section for train operations by using onsite measurement and numerical simulation. J. Wind Eng. Ind. Aerodyn. 174, 69–79.
Ministry of Land, Infrastructure, Transport and Tourism, 2014. http://nlftp.mlit.go.jp/ksj-e/index.html.
Murali, A., Rajagopalan, R.G., 2017. Numerical Simulation of Multiple Interacting Wind Turbines on a Complex Terrain.
Oka, S., Ishihara, T., 2009. Numerical study of aerodynamic characteristics of a square prism in a uniform flow. J. Wind Eng. Ind. Aerodyn. 97, 548–559.
Qi, Y., Ishihara, T., 2018. Numerical study of turbulent flow fields around of a row of trees and an isolated building by using modified k-ε model and LES model. J. Wind Eng. Ind. Aerodyn. 177, 293–305.
Qian, G.-W., Ishihara, T., 2018. A new analytical wake model for yawed wind turbines. Energies 11, 665.
Schulz, C., Klein, L., Weihing, P., Lutz, T., 2016. Investigations into the interaction of a wind turbine with atmospheric turbulence in complex terrain. J. Phys. Conf. Ser. 753, 032016.
Shamsoddin, S., Porté-Agel, F., 2018. Wind turbine wakes over hills. J. Fluid Mech. 855, 671–702.
Shamsoddin, S., Porté-Agel, F., 2017. Large-eddy simulation of atmospheric boundary-layer flow through a wind farm sited on topography. Boundary-Layer Meteorol. 163, 1–17.
Shur, M., Spalart, P.R., Strelets, M., Travin, A., 1999. Detached-eddy simulation of an airfoil at high angle of attack. Eng. Turbul. Model. Exp. 4, 669–678.
Spalart, P.R., Deck, S., Shur, M.L., Squires, K.D., Strelets, M.K., Travin, A., 2006. A new version of detached-eddy simulation, resistant to ambiguous grid densities. Theor. Comput. Fluid Dynam. 20, 181–195.
Wu, Y.T., Porté-Agel, F., 2011. Large-eddy simulation of wind-turbine wakes: evaluation of turbine parametrisations. Boundary-Layer Meteorol. 138, 345–366.
Xian, X., Tao, W., Qingwei, S., Weimin, Z., 2002. Field and wind-tunnel studies of aerodynamic roughness length. Boundary-Layer Meteorol. 104, 151–163.
Yamaguchi, A., Ishihara, T., Fujino, Y., 2003. Experimental study of the wind flow in a coastal region of Japan. J. Wind Eng. Ind. Aerodyn. 91, 247–264.
Yang, X., Howard, K.B., Guala, M., Sotiropoulos, F., 2015. Effects of a three-dimensional hill on the wake characteristics of a model wind turbine. Phys. Fluids 27.